Electronic charge distribution in crystalline germanium

Z. W. Lu
Department of Physics, University of California, Davis, California 95616

Alex Zunger
National Renewable Energy Laboratory, Golden, Colorado 80401

Moshe Deutsch
Department of Physics, Bar Ilan University, Ramat-Gan, 52900, Israel
(Received 10 April 1995; revised manuscript received 18 July 1995)

We use a recently published set of high-accuracy structure factors, based on γ-ray measurements [Dewey *et al.*, Phys. Rev. B **50**, 2800 (1994)] to derive the charge density distribution in crystalline germanium with a millielectron-level resolution. We use a multipole expansion model of the charge densities represented as a superposition of orbital-dependent, nonspherical atomic charge densities. We include in the model anharmonic and nonrigid atomic thermal motions. This model is then fit to the measured structure factors. We find (i) a considerable improvement in the fit residuals (especially for the low-order structure factors) relative to our previous analysis, based on earlier measurements; (ii) a factor-of-2 improvement in the agreement between experiment and our earlier *ab initio* density-functional calculated structure factors; (iii) the evidence for the existence of nonrigid atomic thermal motion is marginal; (iv) a clear $\sim$15% expansion of the valence orbital density relative to the free Ge atom; and (v) a twofold reduced upper limit on the anharmonic force constant. These bring the structure of germanium into better agreement with those of silicon and diamond.

I. INTRODUCTION

Several recent studies of crystalline silicon,[1,2] germanium,[3,4] and diamond,[3,5] demonstrated that the charge distribution in a crystal can be determined to a millielectron level of accuracy, provided that a reasonable number of measured structure factors accurate to $\leq 0.1\%$ is available. This level of accuracy permits analysis[6] of the charge distortions due to bonding, anharmonic corrections to the effective potential and extent of nonrigid atomic thermal motions. We have recently reported an analysis[3] [Lu, Zunger, and Deutsch (LZD)] of the charge distribution in germanium, diamond, and silicon. Our analysis of Ge was based on structure factors measured by Matsushita and Kohra[7] (MK), and Deutsch, Hart, and Cummings[8] (DHC). According to the authors, both sets contained considerable contributions from anomalous dispersion, which could not be accurately corrected for due to the lack of reliable values of the dispersion correction f'. Dewey *et al.*[9] have recently published new γ-ray measurements, done at very high energies, where the contribution of anomalous dispersion is much smaller. Furthermore, they carefully assessed the contribution of f' to their own, and previous, data sets and assembled a dispersion-corrected "best estimate" set of structure factors. We present here a detailed analysis of the charge distribution in germanium, based on this set. The charge distribution derived here shows an overall good agreement with our previous results[3] along with significant improvements in the distribution of the fit residuals, the charge density at the interstitials, and the extent of the agreement with our earlier[3,6] *ab initio* density-functional calculations.

II. METHOD OF ANALYSIS

The analysis here follows that of LZD,[3] which is based on the multipole expansion formalism of Dawson[10] and Stewart.[11] To account for the bonding-induced distortions from the superposition of spherical atomic charge distributions, the crystalline density is expressed here as a sum over lattice sites $\mathbf{r}_j$ of *nonspherical* model densities $R_l K_l$ of angular momenta l, where $R_l(r)$ describes the radial dependence while the Kubic harmonics K_l account for the angular dependence:

$$\rho_{\text{model}}(\mathbf{r}) = \sum_j \sum_{l=0}^{\infty} R_l(|\mathbf{r} - \mathbf{r}_j|) K_l(\hat{r} - \hat{r}_j) \ . \tag{1}$$

Unlike standard x-ray refinements,[12] in which only the lowest, spherical ($l = 0$) term is included we allow here also nonspherical ($l \neq 0$) terms. $R_l(r)$ are represented by

$$\begin{aligned} R_{l=0}(r) &= 4\pi \sum_{nl} \kappa_{nl}^3 \rho_{nl}(\kappa_{nl} r) \ , \\ R_{l=3,4}(r) &= A_l r^{\lambda_l} e^{-\xi r} \ , \end{aligned} \tag{2}$$

where κ_{nl} are the (monopole) expansion/contraction coefficients of the orbital charge density ρ_{nl} contributed

by orbital nl and $\{A_l,\ \lambda_l,\ \xi\}$ are fitting parameters. The static structure factor $\rho_{\rm model}(\mathbf{G})$ at the reciprocal lattice vector $\mathbf{G}$ is obtained from Eq. (1) by Fourier transforming $\rho_{\rm model}(\mathbf{r})$. The dynamic structure factor $F_{\rm model}(\mathbf{G})$ is then given by multiplying $\rho_{\rm model}(\mathbf{G})$ by a temperature factor modeled by LZD in terms of the *orbital-dependent* Debye-Waller factors B_{nl} and the anharmonic force constant β. Thus, the dynamic structure factors $F_{\rm model}(\mathbf{G})$ are expressed in terms of the parameters $\{\kappa_{nl}, \lambda_l, A_l, \xi, B_{nl}, \beta\}$. Fitting $\{F_{\rm model}(\mathbf{G})\}$ to the measured $\{F_{\rm exp}(\mathbf{G})\}$ then provides the values of the unknown parameters and along with them the experimental static charge density $\rho_{\rm model}(\mathbf{r})$ that can be compared with first-principles calculations. The refinement procedure adopted by LZD represents an advance over standard methods not only in that a nonspherical octopole ($l = 3$) and hexadecapole ($l = 4$) density components are included, but also because orbital expansion ($\kappa < 1$) or contraction ($\kappa > 1$) is allowed as is a subdivision of κ and the Debye-Waller factor B into nl =core and nl =valence contributions. The approximations of (i) neglecting all $l > 4$ terms and (ii) using the specific functional form in Eq. (2) were examined and found to be reasonable.

III. SUMMARY OF FITS TO EARLIER DATA

Using calculated,[3] *relativistic* ground-state local-density-approximation[13,14] (LDA) free-atom charge densities $\rho_{nl}(r)$ as input to Eq. (2), our analysis[3] of the earlier experimental data yielded an unweighted R_e factor of $R_e = 0.19\%$, where the "experiment" versus "fit" R_e-factor is defined as

$$R_e = \frac{\sum_{\mathbf{G}} ||\rho_{\rm exp}(\mathbf{G})| - |\rho_{\rm fit}(\mathbf{G})||}{\sum_{\mathbf{G}} |\rho_{\rm exp}(\mathbf{G})|} \ . \qquad (3)$$

We also obtained a goodness of fit (GoF) of 1.07 for the 14 reflections then measured. The available set of $\{F_{\rm exp}(\mathbf{G})\}$ did not allow a confident determination of terms higher than $l = 4$. The fitting parameters of LZD are summarized in the first line of Table I. The resulting experimental valence charge density $\rho_{\rm model}(\mathbf{r})$ is compared with our LDA calculations[3] using the linearized augmented plane wave[15] method as shown in Figs. 1(a) and 1(b). The experimental and LDA-calculated static structure factors are summarized in the first four columns of Tables II and III, which also give $\delta\rho(\mathbf{G}) = \rho_{\rm exp}(\mathbf{G}) - \rho_{\rm fit}(\mathbf{G})$ and $\delta\rho(\mathbf{G}) = \rho_{\rm LDA}(\mathbf{G}) - \rho_{\rm fit}(\mathbf{G})$; the "theory" versus "fit" R factor of LZD was $R_t = 0.37\%$, defined as

$$R_t = \frac{\sum_{\mathbf{G}} ||\rho_{\rm LDA}(\mathbf{G})| - |\rho_{\rm fit}(\mathbf{G})||}{\sum_{\mathbf{G}} |\rho_{\rm LDA}(\mathbf{G})|} \ . \qquad (4)$$

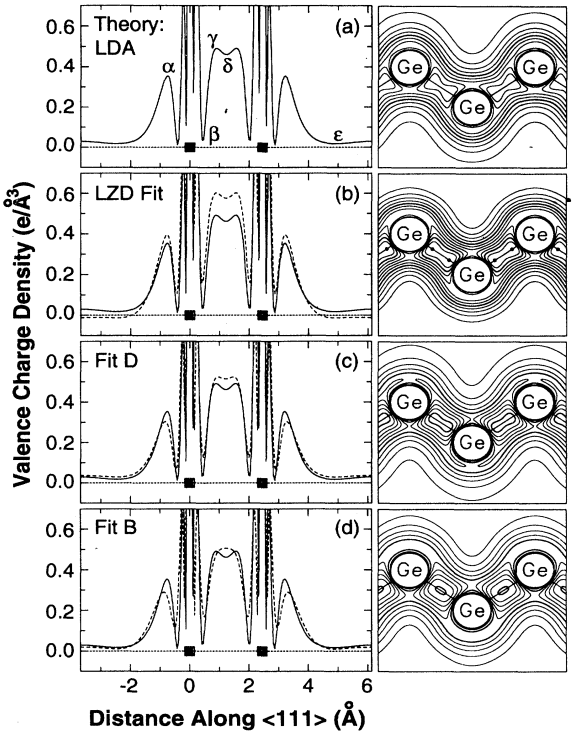

FIG. 1. Valence charge density for Ge as obtained by the (a) *ab initio* LDA theory (Ref. 3) and experiment (b)–(d). The fit of the old (Ref. 3) measured data is given in (b), while the fits to the new data (Table I) are given in (c) and (d). The solid squares denote the atom positions. α, β, γ, and δ indicate special sites along the $\langle 111\rangle$ bond direction, used in Tables IV and V. The dashed lines denote results of the multipole fit to the experimental data while the solid lines (identical in all panels) give the *ab initio* theoretical results. The valence charge density contour maps in the [110] plane are shown to the right, in steps of $0.05e/\text{Å}^3$.

TABLE I. Parameters obtained by fitting Dawson's model [Eqs. (1) and (2)] to the observed structure factors of Ge. In all cases we use in Eq. (2) the relativistic LDA orbitals ρ_{nl} of Ref. 3, and $\lambda_l = 4$ for all l values. An asterisk indicates that the quantity was held fixed during the fit. In fits LZD, A and C we forced $B_{\rm core} = B_{\rm val}$, while in fits B and D we forced $B_{\rm val} = 0$ and let $B_{\rm core}$ vary. An independent variation of both led to $B_{\rm val} \to 0$ and $B_{\rm core} \sim 0.56$ Å^2. For a definition of the various parameters, see text. We list also the R factors of the fits to the measured data, R_e [Eq. (3)], and to the LAPW calculations, R_t [Eq. (4)]. GoF denotes the "goodness of fit" estimator. The LZD fit of the previous data is from Ref. 3. The fit vs experiment R_e in this table was calculated using dynamic structure factors $F(\mathbf{G})$ instead of static structure factors $\rho(\mathbf{G})$.

	κ core	κ valence	ξ a.u.$^{-1}$	A_3 e	A_4 e	$B_{\rm core}$ Å^2	$B_{\rm val}$ Å^2	β eV/Å^3	R_e %	R_t %	GoF
LZD fit	1*	0.9553	1.913	0.583	−0.510	0.5654	0.5654	0.9*	0.19	0.37	1.07
Fit A	1*	0.8300	1.904	0.5293	−0.4648	0.5540	0.5540	0.70*	0.22	0.27	1.19
Fit B	1*	0.8320	1.805	0.5093	−0.4201	0.5566	0.0*	0.38*	0.22	0.27	1.17
Fit C	1*	0.9000*	2.205	0.3758	−0.2834	0.5541	0.5541	0.36	0.24	0.20	1.47
Fit D	1*	0.9000*	2.227	0.3529	−0.2518	0.5572	0.0*	0.00	0.24	0.21	1.48

This is about twice the $R_e = 0.19\%$ value in that study. The comparison between the LZD model and LDA valence charge densities at some special points in the unit cell (denoted α, β, γ, and δ in Fig 1) is given in the first two lines of Table IV, while a similar comparison for the *deformation* density is given in the first two lines of Table V. Table VII summarizes the results obtained for the forbidden reflections.

While the "goodness of fit" of ≈ 1 obtained by LZD shows that the degrees of freedom of the *model* have been exhausted, the real limiting factors were the accuracy of the measured input data $\{F_{\rm exp}(\mathbf{G})\}$ and, in particular, the limited knowledge of the photon-energy-dependent anomalous scattering factor $f'(E,\mathbf{G})$ necessary for correcting $F_{\rm exp}(\mathbf{G})$. Since the MK data[7] was measured at 8 keV, close to the Ge K edge at 11 keV, the f' correction term was about 50-fold larger than the experimental error. Even for the DHC data,[8] measured at 59 keV, f' was about twice the measurement error. It is clear therefore that having reliable values for $f'(E,\mathbf{G})$ is crucial for the determination of the charge distribution from the measured structure factors. Unfortunately, however, no measured f' values were available for Ge at the above-mentioned energies, and the best theoretically calculated values[16] have been shown to differ from experiment by as much as 30–40% for Si.[17]

IV. FITS TO THE "BEST ESTIMATE" DATA SET OF DEWEY *et al.*

Dewey *et al.*[9] (DEA) have recently made an important advance by employing γ rays of energies $E = 342$ and 1382 keV to measure the structure factors of Ge. Such high energies have several advantages. First, the magnitude of $f'(E,\mathbf{G})$ relative to $\rho(\mathbf{G})$ is reduced by more than an order of magnitude as compared to the MK data[7] and so is the influence of inaccuracies in its value. Second, the DEA[9] implementation of the thin plate Laue method,[18,19] permits the use of millimeter, rather than ~ 100 μm, thick crystal plates, relaxing the required tolerances from order of 1 μm to order of 10 μm. Third, the small Bragg angles ($\sim 1°$) render polarization effects negligible and greatly simplify the data analysis. Finally, the commensurate reduction in the rocking curve widths and the increased accuracy and resolution required in the rotation of the plates proved to be well within the interferometric angle measurement capabilities of the sophisticated diffractometer employed in the measurements. It is interesting to notice that the "best value" (111) structure factors of Dewey *et al.* (27.450) are significantly different from the MK value (28.871) and the DHC value (27.904). We use in our refinement below only the DEA value.

To extract the f'-independent static structure factors $\rho_{\rm exp}(\mathbf{G})$, DEA presented a detailed calculation of f'. Due to their high measurement energies, they chose to decompose the dispersion correction as $f'(E,\mathbf{G}) = f'_{\rm LE}(E)+\Delta(\mathbf{G})$, where $f'_{\rm LE}$ is the (low-) energy-dependent anomalous scattering factor and $\Delta(\mathbf{G})$ is the relativistic high-energy limit calculated by Sacchetti[20] and Smith.[21] Values of $f'_{\rm LE}(E)$ for their energies were obtained by fitting the high-order measured structure factors to an expression assuming relativistic Hartree-Fock values for $\rho(\mathbf{G})$ and a Debye parameter of $B = 0.560$ Å^2. The derived f' and B were then used to correct the measured structure factors of DEA,[9] MK,[7] and DHC[8] for dispersion and thermal motion. The three sets were then combined to yield a "best estimate" set of static structure factors $\rho_{\rm exp}(\mathbf{G})$.

Our analysis employs the multipole expansion approach of Eqs. (1) and (2) using these "best estimate" $\rho_{\rm exp}(\mathbf{G})$ as input. The set $\rho_{\rm exp}(\mathbf{G})$ as given in Table VII of Ref. 9 was multiplied back by the Debye-Waller factor $e^{-0.560(\sin\theta/\lambda)^2}$ of DEA[9] to obtain *dynamic* structure factors $F_{\rm exp}(\mathbf{G})$. This set was augmented by the "forbidden" $F_{222} = 0.131 \pm 0.010$ measured by Matsushita and Kohra[7] and Roberto, Batterman, and Keating.[22] This was required to obtain reasonable agreement in the fits with all measured forbidden structure factors. Extensive fits, using different combinations of fixed and refined parameters, were carried out, the results of which are discussed below.

Table I shows the parameters of four of our best fits, denoted A, B, C, and D, along with the parameters obtained by LZD from fitting[3] earlier data. Table II shows the corresponding $\rho_{\rm model}(\mathbf{G})$ from fits A, B, C, and D along with the fit residual $\delta\rho(\mathbf{G}) = \rho_{\rm exp}(\mathbf{G}) - \rho_{\rm fit}(\mathbf{G})$. The following features emerge from the fits:

A. Quality of fits and agreement with LDA

Tables II and III list the static structure factors $\rho_{\rm model}(\mathbf{G})$ obtained from fits A, B, C, and D along with the results $\rho(\mathbf{G})$ of the LZD fit, the experimental values $\rho_{\rm exp}(\mathbf{G})$, and the original *ab initio* LDA results $\rho_{\rm LDA}(\mathbf{G})$. We see from Table III that the discrepancy $\rho_{\rm LDA}(\mathbf{G}) - \rho_{\rm fit}(\mathbf{G})$ at low orders between the old experimental data[7,8] and the LDA calculations has been largely eliminated by the new DEA measurements. The theory versus model R_t factors, which are minimal for fits C and D (Table III), are as small as $R_t = 0.20\%$, almost twofold smaller than $R_t = 0.37\%$ obtained earlier from the LZD model. Similarly, the fit errors $\rho_{\rm exp}(\mathbf{G}) - \rho_{\rm fit}(\mathbf{G})$ (Table II) have been significantly reduced using the DEA data. When compared against the results derived from the *old* experimental set, R_t is reduced by a factor of two, from 0.37% in LZD to 0.20% here (fit C in Table III), while maintaining essentially the same R_e: 0.19% in LZD and 0.24% here (Table I). More significantly, now $R_e \approx R_t$, while using the older experimental data[7,8] LZD found $R_t \sim 2R_e$. This improvement is further demonstrated in Fig. 2, which illustrates the distribution of residuals $\rho_{\rm exp}(\mathbf{G}) - \rho_{\rm fit}(\mathbf{G})$ and $\rho_{\rm LDA}(\mathbf{G}) - \rho_{\rm fit}(\mathbf{G})$, normalized to the experimental uncertainties, σ, for various fits. As can be seen, for the LZD fits the residuals of the low-order reflections are well outside the $\pm 3\sigma$ limits. For the present fits all residuals are within these limits and the errors are more evenly distributed, signifying a better overall fit. The same holds for the residuals relative to

TABLE II. Comparison of the "best estimate" experimental and fitted *static* structure factors $\rho(\mathbf{G})$ for Ge units of e/atom. R_e is the fit vs. experiment R factor [Eq. (3)]. $\delta\rho(\mathbf{G})$ is $\rho_{\rm exp}(\mathbf{G}) - \rho_{\rm fit}(\mathbf{G})$, thirteen values of $\rho(\mathbf{G})$ are used to evaluate R values. The fit vs experiment R_e in this table was calculated using *static* structure factors $\rho(\mathbf{G})$ instead of *dynamic* structure factors $F(\mathbf{G})$ as in Table I, hence there are slight differences. Note that the R_e for LZD is very different from Table I, since we are now comparing with the current "best estimate" data instead of with the old experimental data.

G	exp	LZD		Fit A		Fit B		Fit C		Fit D	
hkl	$\rho_{\rm exp}(\mathbf{G})$	$\rho(\mathbf{G})$	$\delta\rho(\mathbf{G})$	$\rho(\mathbf{G})$	$\delta\rho(\mathbf{G})$	$\rho(\mathbf{G})$	$\delta\rho(\mathbf{G})$	$\rho(\mathbf{G})$	$\delta\rho(\mathbf{G})$	$\rho(\mathbf{G})$	$\delta\rho(\mathbf{G})$
111	27.450	27.894	−0.444	27.468	−0.018	27.442	0.008	27.453	−0.003	27.425	0.025
220	23.581	23.766	−0.185	23.639	−0.058	23.634	−0.053	23.677	−0.096	23.672	−0.091
311	22.181	22.142	0.039	22.128	0.053	22.134	0.047	22.138	0.043	22.144	0.037
222	0.120	0.152	−0.032	0.135	−0.015	0.130	−0.010	0.154	−0.034	0.149	−0.029
400	20.257	20.235	0.022	20.292	−0.035	20.303	−0.046	20.273	−0.016	20.282	−0.025
331	19.606	19.482	0.124	19.532	0.074	19.527	0.079	19.509	0.097	19.505	0.101
422	18.059	18.040	0.019	18.097	−0.038	18.095	−0.036	18.066	−0.007	18.064	−0.005
333	17.345	17.300	0.045	17.351	−0.006	17.349	−0.004	17.315	0.030	17.313	0.032
440	16.173	16.198	−0.025	16.236	−0.063	16.235	−0.062	16.218	−0.045	16.218	−0.045
444	13.528	13.498	0.030	13.497	0.031	13.497	0.031	13.503	0.025	13.502	0.026
660	11.006			10.895	0.111	10.895	0.111	10.909	0.097	10.909	0.097
555	10.669	10.680	−0.011	10.656	0.013	10.656	0.013	10.672	−0.003	10.672	−0.003
777	7.531	7.547	−0.016	7.539	−0.008	7.539	−0.008	7.542	−0.011	7.542	−0.011
R_e%		0.51		0.25		0.24		0.24		0.25	

the LDA calculations, indicating an improved agreement with the *ab initio* calculations as well.

Figure 1 shows the model valence charge density as obtained by our fits of the older data[3] in LZD [Fig. 1(b)] and our present fits to the DEA data [Figs. 1(c) and 1(d)]. Note that the unphysical *negative* density in the interstitial region of the experimental fit in Fig 1(b) has now disappeared [Figs. 1(c) and 1(d)]. As a result the agreement with the *ab initio* results has improved considerably, particularly in the bond region and the side lobes. This can also be seen in Tables IV and V, which compare the valence and deformation densities, respectively, obtained in the fits with $\rho_{\rm model}(\mathbf{r}_i)$ at several special locations $\mathbf{r}_i$ in the unit cell. The deformation density shown in Fig. 3 reveals a considerably improved agreement between theory and experiment in the bond and interstitials regions, although some discrepancy is still observed near the atomic cores. As discussed by LZD,[3] this may reflect the inherently limited flexibility of the multipole expansion, which inhibits a more faithful reproduction of the rapid charge density variations near the core. Note that the presently obtained bond charge map in the [110] plane is more elongated perpendicular to the 111 direction than in LZD, and considerably closer in shape to the theoretical one. The bond charge is also in much better agreement in orientation and shape with those obtained for silicon both theoretically and experimentally (see discussion in Ref. 3).

The results discussed above, showing clear improvement in the distribution of the refinement residuals and a better agreement with the *ab initio* calculations, clearly indicate that the "best estimate" data set of DEA is indeed more consistent internally and of higher accuracy than the previously available partial sets of measured structure factors.

B. Rigid versus nonrigid atomic motion

Fit B uses two different Debye-Waller factors, for the core and valence electrons, with a fixed $B_{\rm val} = 0$. The

TABLE III. Comparison of the LDA-calculated (Ref. 3) and the experimentally fitted static structure factors $\rho(\mathbf{G})$ for Ge in units of e/atom. $\delta\rho(\mathbf{G}) = \rho_{\rm LDA}(\mathbf{G}) - \rho_{\rm fit}(\mathbf{G})$ are the fit residuals and R_t is the corresponding R factor [Eq. (4)], thirteen values of $\rho(\mathbf{G})$ are used to evaluate R values. Table I defines the indicated fits.

G	LDA	LZD		Fit A		Fit B		Fit C		Fit D	
hkl	$\rho_{\rm LDA}(\mathbf{G})$	$\rho(\mathbf{G})$	$\delta\rho(\mathbf{G})$	$\rho(\mathbf{G})$	$\delta\rho(\mathbf{G})$	$\rho(\mathbf{G})$	$\delta\rho(\mathbf{G})$	$\rho(\mathbf{G})$	$\delta\rho(\mathbf{G})$	$\rho(\mathbf{G})$	$\delta\rho(\mathbf{G})$
111	27.519	27.894	−0.375	27.468	0.051	27.442	0.077	27.453	0.066	27.425	0.094
220	23.683	23.766	−0.083	23.639	0.044	23.634	0.049	23.677	0.006	23.672	0.011
311	22.172	22.142	0.030	22.128	0.044	22.134	0.038	22.138	0.034	22.144	0.028
222	0.120	0.152	−0.032	0.135	−0.015	0.130	−0.010	0.154	−0.034	0.149	−0.029
400	20.318	20.235	0.083	20.292	0.026	20.303	0.015	20.273	0.045	20.282	0.036
331	19.432	19.482	−0.050	19.532	−0.100	19.527	−0.095	19.509	−0.077	19.505	−0.073
422	18.016	18.040	−0.024	18.097	−0.081	18.095	−0.079	18.066	−0.050	18.064	−0.048
333	17.275	17.300	−0.025	17.351	−0.076	17.349	−0.074	17.315	−0.040	17.313	−0.038
440	16.187	16.198	−0.011	16.236	−0.049	16.235	−0.048	16.218	−0.031	16.218	−0.031
444	13.493	13.498	−0.005	13.497	−0.004	13.497	−0.004	13.503	−0.010	13.502	−0.009
660	10.924			10.895	0.029	10.895	0.029	10.909	0.015	10.909	0.015
555	10.684	10.680	0.004	10.656	0.028	10.656	0.028	10.672	0.012	10.672	0.012
777	7.543	7.547	−0.004	7.539	0.004	7.539	0.004	7.542	0.001	7.542	0.001
R_t%		0.37		0.27		0.27		0.20		0.21	

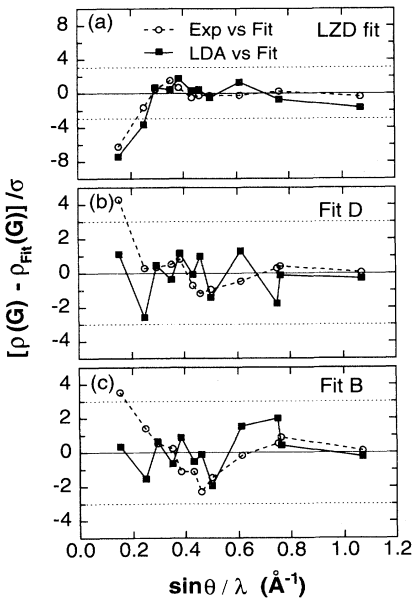

FIG. 2. The normalized fit residuals $\Delta\rho_e = [\rho_{\rm exp}(\mathbf{G}) - \rho_{\rm fit}(\mathbf{G})]/\sigma$ (solid squares and line) and $\Delta\rho_t = [\rho_{\rm LDA}(\mathbf{G}) - \rho_{\rm fit}(\mathbf{G})]/\sigma$ (open circles and dashed line) for (a) the LZD fit (Ref. 3) to the old measured data (Refs. 7 and 8), (b) fit D, and (c) fit B, both to the "best estimate" data of Ref. 9. σ is the experimental uncertainty in the measured values. Note the different scales in (a), (b), and (c), the greatly improved fit for low-order reflections in (b) and (c), and the generally more even distribution of the residuals in the new fits. The dashed lines give the bound of $\pm 3\sigma$.

R_e factors are identical to, and the GoF is slightly better than, those of fit A, which assumes $B_{\rm core} = B_{\rm val}$. More significantly, when two Debye-Waller factors are assumed, and $B_{\rm val}$ and $B_{\rm core}$ are free to vary, $B_{\rm val}$ always goes to zero, while $B_{\rm core}$ converges to a finite, $B_{\rm core} \approx 0.56$ Å^2, value. A similar behavior was found for Si in Ref. 2 (see also Table I in Ref. 3). The rather large 0.11-Å^2 fit uncertainty of $B_{\rm val}$ obtained for silicon was taken there as an upper limit for $B_{\rm val}$, rather than assuming a strict $B_{\rm val} = 0$ Å^2. Here, as there, the $B_{\rm val} \to 0$ obtained reflects a greater, bonding-induced, rigidity of the valence electron structure. However, the accuracy level and limited number of the measured structure factors, as well as the low value of $B_{\rm val}$ do not allow its precise determination from the data even for silicon.

C. Valence shell contraction/expansion

A series of fits were carried out in which the monopole shell parameter $\kappa_{\rm val}$ was successively stepped through fixed values ranging from 0.7 (expansion of 30%) to 1.3 (contraction of 30%), optimizing all other parameters to obtain a best fit. Figure 4 shows the resultant R_e factor and GoF plotted against $\kappa_{\rm val}$. A distinct minimum is obtained close to $\kappa_{\rm val} \sim 0.85$, indicating an *expansion* of $\sim$ 15% of the valence shell. In particular, no indication is found for a minimum in R for $\kappa_{\rm val} \geq 1$ that may indicate a *contraction* of the valence shell, as suggested recently by O'Keeffe and Spence[23] based on average crystal potentials derived from electron diffraction measurements. Our results are, again, in line with earlier studies of silicon[25] (6% expansion) and diamond[3,4] (1% expansion) where valence shell expansions of a few percent were reported.

To examine this point further, we have conducted a similar series of fits of the multipole model to the LDA-*calculated* static structure factors $\rho_{\rm LDA}(\mathbf{G})$. The fit was repeated for increasingly larger sets of structure factors. The results are shown in Table VI. We see that (i) for a small number of structure factors (of the order obtainable in measurements) the LDA results predict orbital expansion for the valence shell, as do the experimental results. The magnitude of the expansion is, however, smaller than that obtained from the limited set of measured structure factors. (ii) As the number N of structure factors is increased (beyond that currently accessible to accurate measurements) the magnitude of the orbital expansion is reduced. A similar trend was observed for Si (Fig. 14 in Ref. 3). (iii) However, even for a very large set of structure factors, the LDA results still predict an orbital *expansion* of $\sim$ 1.5% in germanium. Thus, the measured, as well as the LDA-calculated data do not support the suggestion of O'Keeffe and Spence[23] of solid state orbital *contraction* in these materials.

D. Anharmonic force factor β

The upper limit $\beta < 0.9$ obtained by LZD[3] is now reduced to $\beta \leq 0.5$. This, again, brings Ge in line with the results of LZD for Si and diamond, where a zero anharmonic force constant was obtained. Comparing fits A and C (as well as B and D), we find no significant differences in the agreement for different β values. While

TABLE IV. Values of the valence charge density $\rho_{\rm val}(R)$ (e/Å^3) at special positions $|R|$ (in units of $\sqrt{3}a$, with origin on the left atom of Fig. 1) at various points (α, β, γ, δ, and ϵ) along the ⟨111⟩ direction as indicated in Fig. 1(a).

	α		β		γ		δ		ϵ	
	$\rho_{\rm val}$	$\lvert R\rvert$	$\rho_{\rm val}$	$\lvert R\rvert$	$\rho_{\rm val}$	$\lvert R\rvert$	$\rho_{\rm val}$	$\lvert R\rvert$	$\rho_{\rm val}$	$\lvert R\rvert$
LZD Fit	0.40	0.079	0.16	0.042	0.60	0.092	0.58	0.125	−0.01	0.50
LDA	0.36	0.077	0.02	0.044	0.49	0.091	0.46	0.125	0.02	0.50
Fit B	0.29	0.089	0.17	0.047			0.51	0.125	0.01	0.50
Fit D	0.30	0.084	0.13	0.047	0.52	0.097	0.51	0.125	0.03	0.50

TABLE V. Values of the total deformation density $\Delta\rho_{\rm tot}(R)$ (in units of $e/\text{Å}^3$) and $|R|$ (in units of $\sqrt{3}a$) at the same points as in Table V along the $\langle 111\rangle$ direction as indicated in Fig. 4(a).

	α		β		δ		ϵ	
	$\rho_{\rm val}$	$\lvert R\rvert$	$\rho_{\rm val}$	$\lvert R\rvert$	$\rho_{\rm val}$	$\lvert R\rvert$	$\rho_{\rm val}$	$\lvert R\rvert$
LZD Fit	−0.01	0.068	0.09	0.057	0.25	0.125	−0.05	0.50
LDA	−0.05	0.076	−0.06	0.051	0.13	0.125	−0.02	0.50
Fit B	−0.16	0.069	−0.08	0.062	0.17	0.125	−0.02	0.50
Fit D	−0.13	0.069	−0.02	0.062	0.18	0.125	−0.00	0.50

this means that there is no support for a finite, nonzero β, it also does not exclude one as long as it is small, as discussed above. This conclusion is also supported by the recent powder study of Saravanan, Mohanlal, and Nethaji.[24]

E. Forbidden reflections

The nonzero values of the "forbidden" structure factors are contributed solely by the antisymmetric component of the bonding charge, R_3K_3, and the anharmonic force constant β seen by the centrosymmetric charge components R_0 and R_4K_4. A comparison of the *ab initio* calculated, and the multipole expansion, values with the measured ones provides therefore important tests for the quality of the calculation and the fitted models. Due to their small magnitude, only the three lowest-order such factors were ever measured for Ge: F_{222}, F_{442}, and F_{622}. The values obtained for these in the various fits and in the LDA calculations are given in Table VII, along with the measured[7,26,27] values and those obtained by LZD. Note that the measured F_{222} was included in the fit, while the other two were not. The overall agreement of the fits is reasonable, with fits A and B showing a better agreement with the measured $F_{222} = 0.133$ than that of LZD fit (0.147). The LDA results for F_{222} (0.114) underestimates the measured and fitted values, as noted previously.[3] The LDA values for F_{442} and F_{622} (~ 2 me) are probably within the computational error. The multipole fit results for F_{442} are in fair agreement with the two measurements,[26,28] which, however, differ by $\sim 40\%$. The two[26,28] measured F_{622} values are in better agreement with each other, but are considerably underestimated by all fit values. Note that fits B and D, which assume $B_{\rm val} = 0$, are systematically lower than A and C, which assume $B_{\rm val} = B_{\rm core}$. This brings the A and C F_{622} results to a slightly better agreement with experiment than B and D, which argues for a rigid atomic thermal motion. The significant difference in the two measured F_{442} values, however, does not allow a similar comparison for this structure factor.

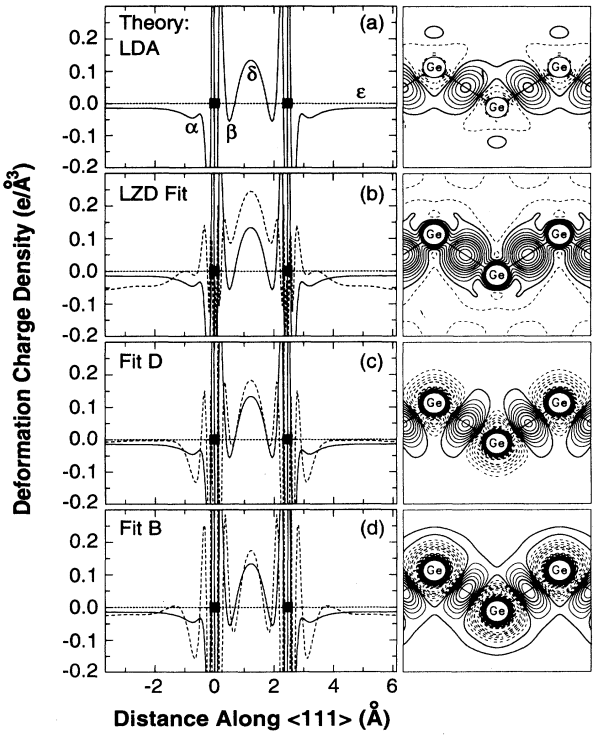

FIG. 3. Deformation charge density for germanium. The thick solid contour denotes $\Delta\rho = 0$. Dashed contours denote negative $\Delta\rho$. The contour steps are $0.025e/\text{Å}^3$. Solid lines, identical in all panels, are the theoretical LDA results, while the dashed lines are from fits to the experimental data. For further notation see caption to Fig. 1.

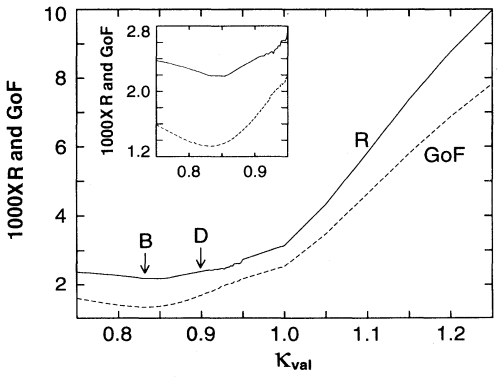

FIG. 4. The R_e-factor [Eq. (3)] and the GoF estimators for the multipole model fits to the "best estimate" structure factor vs the valence expansion/contraction parameter $\kappa_{\rm val}$. The region of the minima is enlarged in the inset. Arrows indicate the fits of B and D.

TABLE VI. The valence shell expansion/contraction parameter $\kappa_{\rm val}$ obtained by fitting the LDA-calculated static structure factors $\rho_{\rm LDA}(\mathbf{G})$ by the multipole model in Eqs. (1) and (2) for lattice vectors up to the indicated $\mathbf{G}_{\rm max}$ [denoted by the corresponding $(\sin\theta/\lambda)_{\rm max}$]. N is the number of structure factors within this limit. Negative values indicate expansion. The fit to 13 *measured* structure factors yields values of -10% to -17%, as shown in Table I.

$(\sin\theta/\lambda)_{\rm max}$ (Å^{-1})	N	$(1-\kappa_{\rm val})\times 100$ (%)
0.4	8	-7.5
0.6	18	-4.5
0.8	35	-4.0
0.9	46	-3.0
1.0	59	-2.5
1.2	96	-2.0
1.4	139	-2.0
1.6	198	-1.5
1.8	271	-1.5
2.0	357	-1.5
2.1	411	-1.5

TABLE VII. Multipole fit and LAPW-calculated dynamic structure factors $F(\mathbf{G})$ (using $B = 0.5654$ Å^2) for the "forbidden" reflections $h+k+l = 4n \pm 2$ in electron units. The model fits are defined in Table I.

		F_{222}	F_{442}	F_{622}
Ab initio theory	LDA	0.1135	0.0026	0.0020
Multipole model fit	LZD fit[a]	0.1466	0.0116	0.0056
	Fit A	0.1304	0.0098	0.0047
	Fit B	0.1314	0.0078	0.0032
	Fit C	0.1469	0.0111	0.0041
	Fit D	0.1485	0.0097	0.0027
Experiment	MK[b]	0.1330		
	MB[c]		0.0079	0.0070
	TB2[d]		0.0123	0.0083

[a]Reference 3.
[b]Reference 7.
[c]Reference 26.
[d]Reference 28.

V. SUMMARY

The analysis based on the new γ-ray measurements of Dewey *et al.*[9] shows the following: (i) The experiment versus model R factor R_e is essentially the same as the LZD fit to the older data, but the fit residuals for the lowest-order structure factors are considerably smaller here, indicating a better fit. (ii) The static density $\rho_{\rm model}(r)$ obtained from the fit shows a factor of two improvement in the agreement with the *ab initio* LDA calculations, bringing R_e and R_t into equality. Furthermore, the unphysical *negative* valence densities found previously by LZD in the interstitial region of the valence density of $\rho_{\rm model}(r)$ have now disappeared, and the agreement with theory in the bond region is improved. (iii) No support is obtained for a nonrigid thermal motion, in line with the conclusions of LZD. However, now the single $B = 0.5541$ Å^2, slightly down from $B = 0.5654$ Å^2 of LZD, but in very good agreement with Ref. 8. (iv) The expansion of the valence shell, found in LZD is reconfirmed, albeit with a larger magnitude of 10%–17% ($\kappa_{\rm val} \sim 0.9 - 0.83$) as compared to a 4.5% ($\kappa_{\rm val} = 0.955$) of LZD. (v) Finally, the upper limit on the anharmonic force constant $\beta < 0.9$ found by LZD is now further reduced to $\beta \leq 0.5$.

ACKNOWLEDGMENTS

Z.W.L. thanks the University Research Funds of the University of California at Davis for support. A.Z. acknowledges support of the Office of Energy Research (OER) [Division of Materials Science of the Office of Basic Sciences (BES)], U. S. Department of Energy, under Contract No. DE-AC36-83CH10093. M.D. gratefully acknowledges the support of the Bar-Ilan Research Authority.

[1] P.F. Price, E. N. Maslen, and S. L. Mair, Acta Crystallogr. Sect. A **34**, 183 (1978); M. A. Spackman, *ibid.* **42**, 271 (1986).
[2] M. Deutsch, Phys. Rev. B **45**, 646 (1992); **46**, 607 (1992).
[3] Z. W. Lu, A. Zunger, and M. Deutsch, Phys. Rev. B **47**, 9385 (1993).
[4] A. S. Brown and M. A. Spackman, Acta Crystallogr. Sect. A **46**, 381 (1990).
[5] M. A. Spackman, Acta Crystallogr. Sect. A **47**, 420 (1991).
[6] Z. W. Lu and A. Zunger, Acta Crystallogr. Sect. A **48**, 545 (1992).
[7] T. Matsushita and K. Kohra, Phys. Status Solidi **24**, 531 (1974).
[8] M. Deutsch, M. Hart, and S. Cummings, Phys. Rev. B **42**, 1248 (1990).
[9] M. S. Dewey, E. G. Kessler, G. L. Greene, D. Deslattes, F. Sacchetti, C. Petrillo, A. Freund, H. G. Böner, S. Robinson, and P. Schillebeecks, Phys. Rev. B **50**, 2800 (1994).
[10] B. Dawson, Proc. R. Soc. London **298**, 264 (1967); **298**, 379 (1967).
[11] R. F. Stewart, J. Chem. Phys. **58**, 1668 (1973); Acta Crystallogr. Sect. A **32**, 565 (1976).
[12] *Electron and Magnetization Densities in Molecules and Crystals*, edited by P. Becker (Plenum, New York, 1980).
[13] P. Hohenberg and W. Kohn, Phys. Rev. **136**, B864 (1964).
[14] W. Kohn and L. J. Sham, Phys. Rev. **140**, A1133 (1965).
[15] D. J. Singh, *Planewaves, Pseudopotentials, and the LAPW Method* (Kluwer, Boston, 1994).
[16] D. T. Cromer, Acta Crystallogr. **18**, 17 (1965); D. T. Cromer and D. J. Liberman, J. Chem. Phys. **53**, 1891 (1970).
[17] D. C. Creagh, Aust. J. Phys. **41**, 487 (1988); M. Deutsch and M. Hart, Phys. Rev. B **30**, 640 (1984); **37**, 2701 (1988).
[18] R. Teworte and U. Bonse, Phys. Rev. B **29**, 2102 (1984).
[19] M. Deutsch and M. Hart, Phys. Rev. B **31**, 3846(1985); Acta Crystallogr. Sect. A **41**, 48 (1985).

[20] F. Sacchetti, Phys. Rev. B **36**, 3147 (1987).
[21] D. Y. Smith, Phys. Rev. A **35**, 3381 (1987).
[22] J. B. Roberto, B. W. Batterman, and D. T. Keating, Phys. Rev. B **9**, 2590 (1974).
[23] M. O'Keeffe and J. C. H. Spence, Acta Crystallogr. Sect. A **50**, 33 (1994).
[24] R. Saravanan, S. K. Mohanlal, and M. Nethaji, Phys. Status Solidi A **183**, 359 (1994).
[25] P. J. E. Aldred and M. Hart, Proc. R. Soc. London Ser. A **332**, 223 (1973); S. Cummings and M. Hart, Aust. J. Phys. **41**, 423 (1988).
[26] D. Mills and B. W. Batterman, Phys. Rev. B **22**, 2887 (1979).
[27] P. Trucano and B. W. Batterman, Phys. Rev. B **6**, 3659 (1972).
[28] J. Z. Tischler and B. W. Batterman, Phys. Rev. B **30**, 7060 (1984).